Publications

4-23-2019

Artificial Aurora Produced by HAARP

B. Tulegenov
Embry Riddle Aeronautical University, TULEGENB@my.erau.edu

A. V. Streltsov
Embry-Riddle Aeronautical University, streltsa@erau.edu

E. Kendall
SRI International

M. McCarrick
Naval Research Laboratory

I. Galkin
University of Massachusetts Lowell

Scholarly Commons Citation

Correspondence to:
B. Tulegenov,
tulegenb@my.erau.edu

Artificial Aurora Produced by HAARP

B. Tulegenov[1] , A. V. Streltsov[1] , E. Kendall[2] , M. McCarrick[3] , and I. Galkin[4]

[1]Department of Physical Sciences, Embry-Riddle Aeronautical University, Daytona Beach, FL, USA, [2]SRI International, Menlo Park, CA, USA, [3]Naval Research Laboratory, Washington, DC, USA, [4]Center for Atmospheric Research, University of Massachusetts Lowell, Lowell, MA, USA

Abstract We present results from the ionospheric heating experiment conducted at the High Frequency Active Auroral Research Program (HAARP) facility, Alaska, on 12 March 2013. During the experiment, HAARP transmitted in the direction of the magnetic zenith X-mode 4.57-MHz wave. The transmitted power was modulated with the frequency of 0.9 mHz, and it was pointed on a 20-km spot at the altitude of 120 km. The heating (1) generates disturbances in the magnetic field detected with the fluxgate magnetometer on the ground and (2) produces bright luminous spots in the ionosphere, observed with the HAARP telescope. Numerical simulations of the 3-D reduced magnetohydrodynamic (MHD) model reveal that these effects can be related to the magnetic field-aligned currents, excited in the ionosphere by changing the conductivity in the E region when the large-scale electric field exists in the heating region.

1. Introduction

Experiments involving ionospheric heating with high frequency (HF) electromagnetic waves have been conducted on several heating facilities in Europe, Russia, and the United States for more than 60 years. They demonstrate many interesting linear and nonlinear effects observed on the ground, in the ionosphere, and in the magnetosphere of the Earth. Comprehensive reviews of these experiments and their results are given by Gurevich (2007) and Streltsov et al. (2018).

One particular direction of these experiments is a generation of artificial luminous structures in the ionosphere. Actually, the creation of an artificial luminosity was the main goal of one of the first heating facilities constructed in the Soviet Union in 1961 (Gurevich, 2007). A comprehensive review of early experiments focusing on an excitation of optical emissions at the European Incoherent Scatter Scientific Association (EISCAT) and the High Frequency Active Auroral Research Program (HAARP) facilities is given by Kosch et al. (2007).

In general, the heating can be conducted with O-mode or X-mode waves. The more frequently used is the O-mode heating. Usually, the frequency of the O-mode pump wave is chosen close to the maximum frequency of the $F2$ ionospheric region, and the electrons in this region are energized via an anomalous absorption mechanism. This is a "local" heating, and all the effects observed in this case are produced by the increase in the electron temperature at this altitude. This heating can create various luminous structures (in particular, rings and solid spots; Bernhardt et al., 1988, 1989; Pedersen et al., 2009) and artificial ionization layers, which have been studied by Kosch et al. (2005), Mishin et al. (2004, 2005, 2016), and Pedersen et al. (2010).

Another approach to the ionospheric modification is the heating with X-mode HF waves. The X-mode HF waves can interact with the electrons through the cyclotron resonance, and this heating is used to change the temperature of the bulk population of electrons in the ionospheric D and E regions. The variations in the electron temperature change the Hall and Pedersen conductances in the ionosphere. And if there is an electric field in the ionosphere, then the changes in the conductances cause changes in the Hall and Pedersen currents flowing in the ionosphere, which, in turn, generate magnetic field-aligned currents (FACs) flowing into the magnetosphere. This is a so-called Getmantsev's effect (Getmantsev et al., 1974), which was introduced in 1974 and extensively used after that for the generation of ultra-low frequency (ULF) and very-low frequency (VLF) waves in the high-latitude ionosphere-magnetosphere system. The auroral and subauroral zones are particularly favorable for this mechanism because, normally, there is a large-scale electric field in the ionosphere associated with the electrojet (Gurevich, 1978; Robinson et al., 1998; Stubbe & Kopka, 1977;

Stubbe et al., 1981). The injection of extremely-low frequency (ELF)/VLF waves into the magnetosphere via modulated heating of the electrojet by HAARP has been extensively studied by Papadopoulos et al. (2003), (Golkowski et al., 2008, 2011), and Cohen et al. (2010).

If the frequency of the ULF wave generated with heating matches one of the eigenfrequencies of the global magnetospheric resonator, then this wave can form a standing pattern along the magnetic field line between the conjugate hemispheres. In this case, a large-amplitude ULF wave can be generated by a relatively small ionospheric disturbance modulated with the eigenfrequency of the resonator (e.g., Streltsov et al., 2005). The large-amplitude ULF Alfvén waves may have a parallel electric field due to kinetic or inertial wave dispersion (Goertz & Boswell, 1979; Hasegawa, 1976), anomalous resistivity (Mozer, 1976), plasma turbulence (Jasperse et al., 2010), mirror force (Nakamura, 2000), and so forth. This electric field can accelerate electrons along an ambient magnetic field into the ionosphere and cause bright, discrete auroral forms. The causal connection between magnetic FACs carried by shear Alfvén waves and natural luminous auroral structures has been convincingly demonstrated in many studies reviewed by Stasiewicz et al. (2000). At the same time, there are still not many successful experiments reported in the literature, where the heating of the ionosphere with X-mode waves simultaneously produces disturbances in the magnetic field and the artificial airglow. In this paper we reproduce with 3-D MHD simulation results from one of the first successful experiments devoted to this problem.

2. The HAARP Heating Experiment

The experiment was conducted at HAARP on 12 March 2013 from 06:45 to 08:00 UT (corresponding to 11 March 2013, 22:45–24:00 Alaskan Daylight Time). During the experiment, HAARP transmitted X-mode electromagnetic waves with a frequency of 4.57 MHz in the direction of the local magnetic zenith (or in the direction of the ambient magnetic field). It has been shown in many studies, for example, (Honary et al., 2011; Rietveld et al., 2003; Streltsov et al., 2018), that heating in the magnetic zenith (MZ) is the most efficient for changing the electron temperature in the ionosphere. The size of the heated spot at the altitude of 120 km for the 3-dB beam width of 4.57-MHz vertical beam is ≈20 km. The spot does not change its location during the entire experiment. The total power of the HAARP transmitter was 3.6 MW. The effective radiated power of the transmitter is 1,023 MW for the 4.57-MHz wave. The change in the beam direction from vertical to the MZ (≈14.4° at HAARP magnetic latitude) may cause insignificant (≈3%) change in the size of the heating spot in the ionosphere and small variation in the effective radiated power.

The HF signal has been modulated with a 0.9-mHz (556-s ON/OFF) frequency. This frequency was chosen from the observations of large-amplitude ULF waves detected with the fluxgate magnetometer in Gakona, Alaska, during several experimental campaigns at HAARP in the years 2011–2013 (Guido et al., 2014). These observations frequently demonstrate waves with frequencies of 0.75 and 0.9 mHz during the periods of strong geomagnetic disturbances. These frequencies are at the low end of the so-called "magic" frequencies, sometimes attributed to shear Alfvén waves standing inside the global magnetic field resonator (Fenrich et al., 1995; Samson et al., 1992).

During the experiment, three components of the magnetic field have been measured with the HAARP fluxgate magnetometer in Gakona. The blue line in Figure 1a shows the D-component of the magnetic field, measured by the fluxgate magnetometer in Gakona on 12 March 2013 from 05:30 to 09:30 UT. The black line in Figure 1a shows the low-frequency (<0.7 mHz) part of the signal, and Figure 1b shows the high-frequency (>0.7 mHz) part. The vertical red lines in Figures 1a and 1b mark the time of the beginning and the ending of the experiment. The time when the transmitter was ON is marked with pink boxes in Figure 1b.

Figure 1c shows the power spectral density of the signal shown in Figure 1b in the frequency range from 0 to 5 mHz. Figure 1c shows that the main power of the signal is in the frequency of modulation 0.9 mHz, and Figure 1b shows very good correlation in phase and frequency between the periodicity of the heater's ON/OFF intervals and the oscillations of the magnetic field measured on the ground. The H-component of the magnetic field measured by the magnetometer during this time interval also reveals oscillations with the frequency of 0.9 mHz (not shown in the paper). These results suggest that X-mode heating indeed generates ULF waves and magnetic FACs, as was previously suggested by Blagoveshchenskaya et al. (2001) and Streltsov et al. (2012).
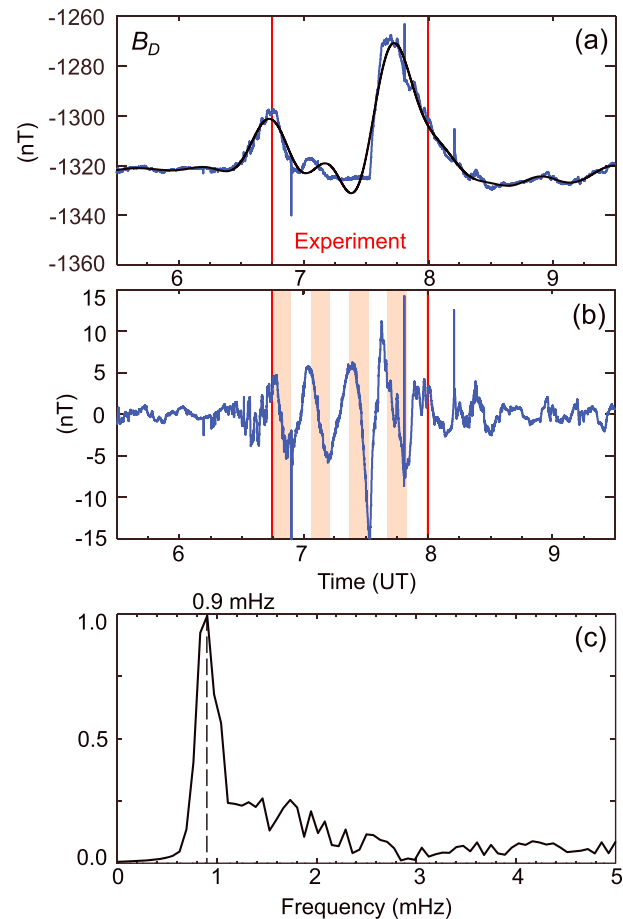
Figure 1. (a) The blue line shows the D-component of the magnetic field, B_D, measured by the fluxgate magnetometer in Gakona on 12 March 2013. The black line shows the low-frequency (≤ 0.7 mHz) part of the signal. (b) High-frequency (≥ 0.7 mHz) part of the B_D shown in panel (a). (c) Normalized power spectral density of B_D shown in panel (b).

Figure 2 shows three sets of 630.0-nm optical images taken during the experiment by the HAARP telescope. The telescope can take images in 427.8 nm, 557.7-, 630.0-, and 777.4-nm wavelengths. The first set of images was taken during the time interval 06:45:00–06:54:15 UT, when the heater was ON. This set contains images with a bright luminous spot in the center. The second set of images was taken during time interval 06:54:15–07:03:31 UT, when the heater was turned OFF and no luminosity was observed. The third set of images was taken during the time interval 07:03:31–07:12:46 UT, when the heater was ON, and this set again shows a luminous spot in the ionosphere. Thus, the observations with 630.0-nm filter demonstrate optical emissions during the first two (out of total four) time intervals when the heater was ON.

Observations with 557.7-nm filter demonstrate optical emissions during the same time intervals as well, although the structures of the emissions in 557.7-nm wavelength are different compared to the ones observed in 630.0-nm wavelength. For comparison, Figure 3 shows two high-resolution images in 630.0- and 557.7-nm wavelengths at times 06:53:28 and 06:53:32 UT correspondingly. The main difference between these two images is that 630.0-nm luminosity is relatively smooth and 557.7-nm image is more "structured" as was observed previously by Pedersen et al. (2010).

3. Model and Numerical Implementation

The 3-D two-fluid reduced MHD model has been described in detail in several papers devoted to the electrodynamic coupling between the ionosphere and the magnetosphere at high latitudes (Jia & Streltsov, 2014; Streltsov & Pedersen, 2011), and it is mentioned here only for completeness. The magnetospheric part of the model consists from electron parallel momentum equation

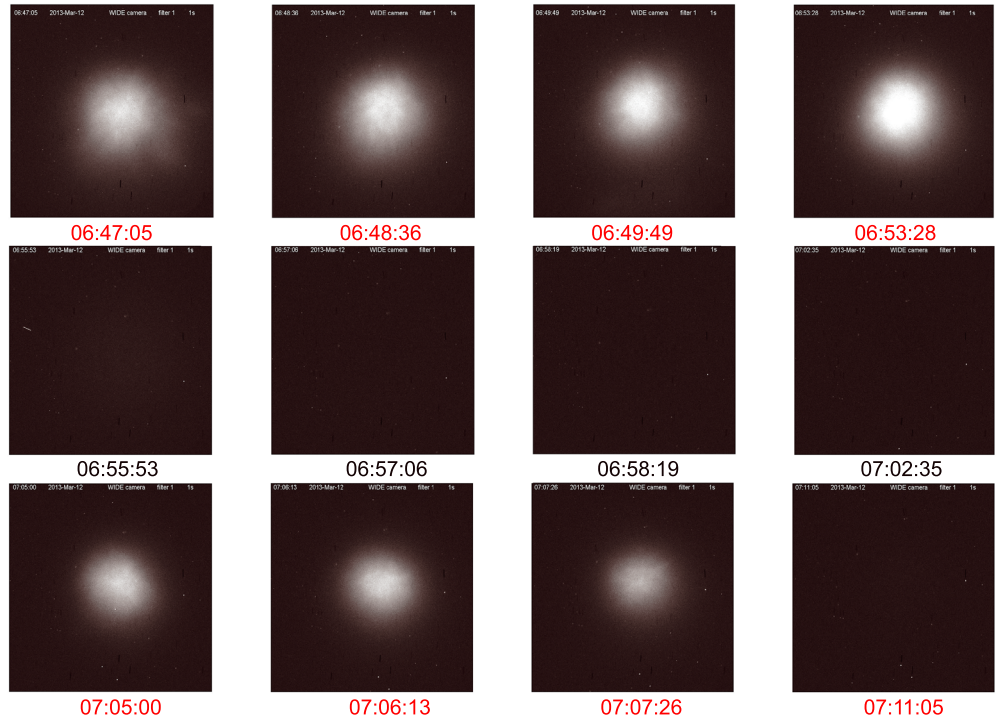March 12, 2013   06:45:00 - 06:54:15 ON; 06:54:15 - 07:03:31 OFF; 07:03:31 - 07:12:46 ON   630.0 nm

Figure 2. Series of images of the artificial aurora created by High Frequency Active Auroral Research Program in 630.0-nm wavelength.

$$\frac{\partial v_{\|e}}{\partial t} + v_{\|e}\nabla_{\|}v_{\|e} + \frac{e}{m_e}E_{\|} + \frac{1}{m_e n_0}\nabla_{\|}(nT_e) = -f_e v_{\|e}, \tag{1}$$

the current continuity equation

$$\nabla \cdot \left[\left(\frac{1}{v_A^2} + \frac{1}{c^2} \right) \frac{\partial E_\perp}{\partial t} \right] = \mu_0 \nabla \cdot (j_{\|} \mathbf{b}), \tag{2}$$

and the density continuity equation

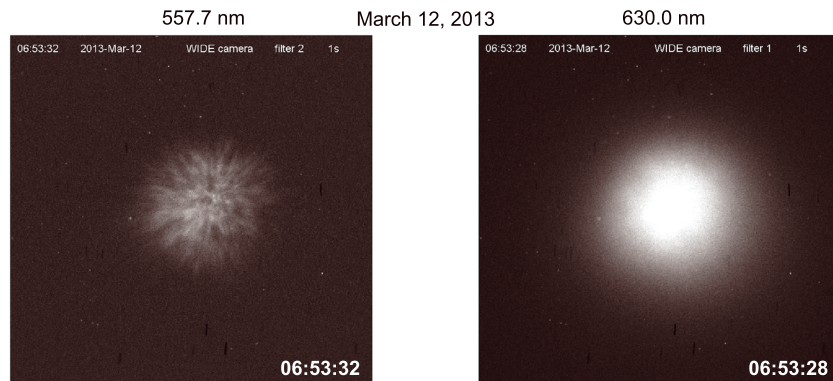$$\frac{\partial n}{\partial t} = -\nabla \cdot (n v_{\|e} \mathbf{b}). \tag{3}$$

Figure 3. Images of the artificial aurora created by High Frequency Active Auroral Research Program in 557.7-nm wavelength (left) and 630.0-nm wavelength (right).

where subscripts $\parallel$ and $\perp$ indicate parallel and perpendicular vector components to $\mathbf{b} = \mathbf{B}_0/B_0$, respectively, v_e is the electron velocity, n_0 is the background quasi-neutral plasma density, T_e is the background electron temperature, f_e is the electron collision frequency, $v_A = B_0/(\mu_0 n_0 m_i)^{0.5}$ is the Alfvén speed, and m_i is the proton mass. The electron temperature is modeled as $T_e = (T_{e*}n_*)/n_0$, where $T_{e*} = 200$ eV and n_* is the density at the equator. Such an assumption satisfies the equilibrium condition $\nabla_z(n_0 T_e) = 0$.

The constant heating of the ionosphere by HAARP is modeled by solving simultaneously the highly integrated density continuity equation with the reduced recombination in the northern ionosphere

$$\frac{\partial n}{\partial t} = \frac{j_\parallel}{eh} + \alpha \left(n_0^2 - (1-H)n^2 \right),$$

(4)

and the current continuity equation in the ionosphere,

$$\nabla \cdot \left(\Sigma_P \mathbf{E}_\perp + \Sigma_H \mathbf{E}_\perp \times \mathbf{b} \right) = \pm j_\parallel.$$

(5)

Here, $\Sigma_P = M_P nhe/\cos\lambda$ and $\Sigma_H = M_H nhe/\cos\lambda$ are the height-integrated Pedersen and Hall conductivities; $M_P = 10^4$ m^2/sV is the ion Pederson mobility, and M_H is the Hall mobility; $h = 20$ km is the effective thickness of the E region; λ is the angle between the normal to the ionosphere and the corresponding dipole magnetic field line at 120-km altitude, and $\alpha = 3 \times 10^7$ cm^3/s is the recombination coefficient. The sign "+" in (5) is used in the Southern Hemisphere, and the sign "−" is used in the Northern Hemisphere.

H in (4) specifies the heating. It is chosen as $H = 0.5 \exp[-(\rho/\rho_0)^2]$, where ρ is the distance in the ionosphere from the location of the maximum of the heater beam and $\rho_0 = 10$ km is a half-width of the beam. Experiments with HF X-mode heating have shown that the density can be enhanced by up to 70% relative to the background (Blagoveshchenskaya et al., 2015). We assume that the heater modifies the density by 20%, which is well within the reported values.

The model equations are written in the orthogonal dipole coordinates (L, ϕ, μ), where $L = r\sin^2\theta$, $\mu = \cos\theta/r^2$, and r, θ, and ϕ are standard spherical coordinates. Computations have been performed in the three-dimensional dipole magnetic flux tube bounded by the ionosphere in the Northern and Southern Hemispheres. The latitudinal boundaries of the domain are formed by $L = 4.75$ and $L = 5.05$ magnetic shells. The azimuthal size of the domain is $\phi \approx 1°$. The computational grid inside the domain has 101 steps in the L direction, 64 steps in the ϕ direction, and 101 steps in the μ direction. The steps are uniform in the L and ϕ directions and strongly nonuniform in the μ direction. In particular, the size of steps in the μ direction decreases 200 times from the equator to the ionosphere, and, as a result, the grid is denser at low altitudes and sparser in the equatorial magnetosphere. Periodic boundary conditions are implemented on the boundaries in the ϕ direction, and the Dirichlet's boundary conditions are implemented on the boundaries in the L direction.

3.1. Background Parameters

The geomagnetic field is defined as $B_0 = B_*(1 + 3\sin^2\theta)^{0.5}/r^3$, with $B_* = 31,000$ nT and r is a geocentric distance given in $R_E = 6371.2$ km. The magnitude of the large-scale $E_\perp$ is based on the digisonde drift velocities presented in Figure 4. Using the two components of the electron drift velocity, we calculate the resultant $E_\perp$. The amplitude of the electric field during the first two periods of the heating was peaking at 6.5 mV/m at 06:50 UT. After 07:15 UT, the magnitude of the large-scale $E_\perp$ decreases and reaches a minimum of 2.85 mV/m at 07:45 UT.

The profile of the background density along $L = 4.90$ magnetic field line (corresponding to the location of HAARP) is defined as

$$n_0 = \begin{cases} a_1(r - r_1) + a_2, & \text{if } r_1 < r < r_2 \\ b_1 e^{-20(r-r_2)} + b_2 r^{-4} + b_3, & \text{if } r > r_2. \end{cases}$$

(6)

Here r is the radial distance to point on the field line, $r_1 = 1 + 120/R_e$, and $r_2 = 1 + 320/R_e$. The constants a_1, a_2, b_1, b_2, and b_3 are parameters that satisfy a density of 1.25×10^4 cm^{-3} at E region altitude of 120 km, 1.5×10^5 cm^{-3} at F region altitude of 320 km, and 129 cm^{-3} in the equatorial magnetosphere.
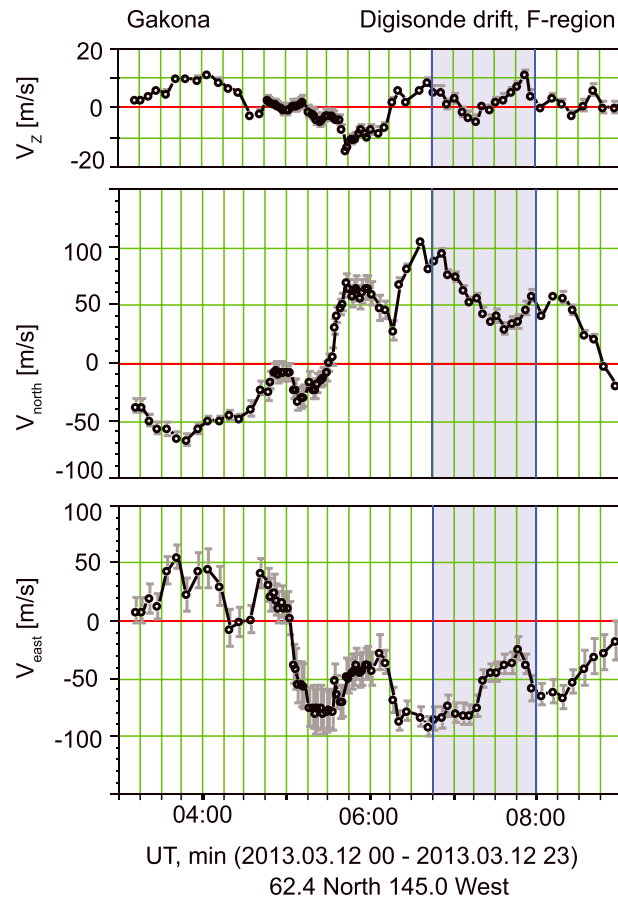
Figure 4. Electric field in the ionosphere above High Frequency Active Auroral Research Program during the experiment.

One of the main parameters in the model is the density in the ionospheric *E* region. That density defines the conductivities of the ionosphere, which are supposed to be modified by the heating. Data from the HAARP digisonde, shown in Figure 5, demonstrate that this density is quite low. At the least, it is below the threshold which can be detected by the digisonde. Because the digisonde can detect densities starting from 1.25×10^4 cm^{-3} (corresponding to the plasma frequency of 1 MHz), we decided to choose this value for the magnitude of the background density in the simulations. This value of the density provides $\Sigma_P = 0.4$ mho.

4. Results and Discussion

The experiment conducted at HAARP on 12 March 2013 brings two equally important and interesting results. First, it demonstrates, for the first time, that heating of the ionosphere with X-mode HF waves can generate bright luminous structures in 557.7-, 630.0-, and 777.4-nm wavelengths. On the other hand, there were no luminous structures observed in the 427.8-nm wavelength (higher energy blue line). Figure 2 shows three sets of optical images in 630.0-nm wavelength taken with the HAARP telescope during the experiments. It is worth mentioning here that normally, the airglow has been observed in the ionosphere above HAARP only during the O-mode heating (Kosch et al., 2005).

Of course, the X-mode heater transmissions always contain some level of contaminating O-mode polarization. However, the HAARP array controls and monitors the currents on each dipole independently and can maintain very high isolation between polarizations. In this case, the measured O-mode component was at least 25 dB below the X-mode level. Furthermore, the sequence of ionograms presented in Figure 5 shows that the highest frequency reflected by O-mode transmission, including the considerable frequency spread, was no greater than 4 MHz, well below the heating frequency of 4.57 MHz used in this experiment, while *fxF*2 exceeded the heating frequency prior to 07:20 UT.
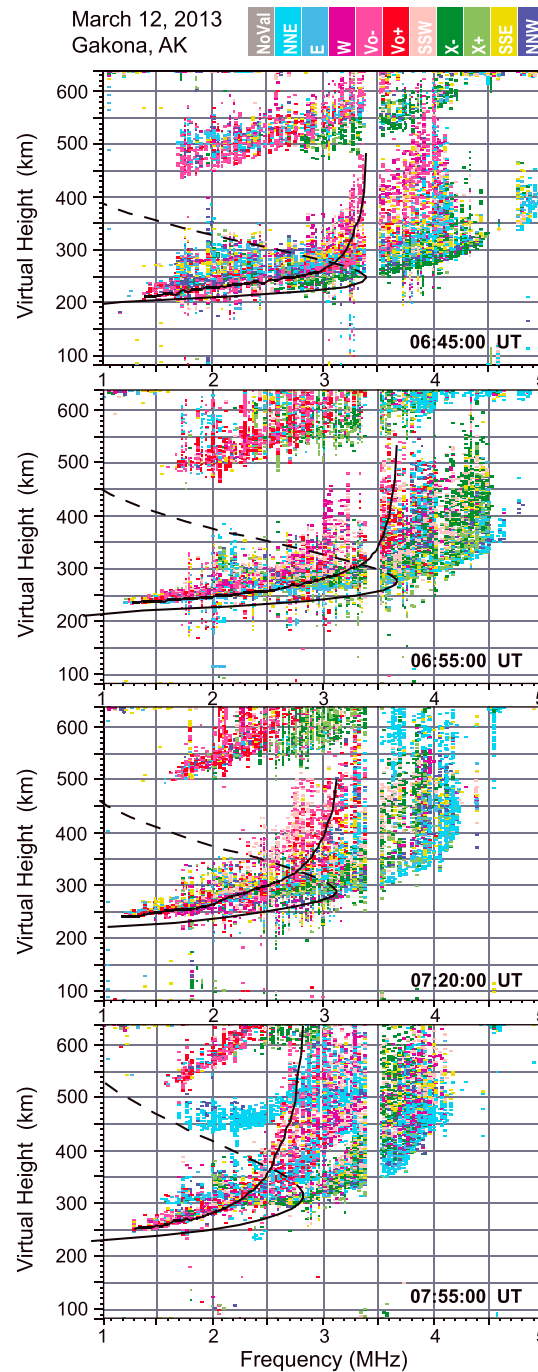
Figure 5. Ionospheric density above High Frequency Active Auroral Research Program during the experiment.

Second, the 12 March 2013 experiment generates oscillations in the magnetic field with the frequency perfectly matching the frequency of heating modulations. These observations are shown in Figure 1b, which gave a strong reason to conclude that during the experiment HAARP indeed produces magnetic FACs flowing into the magnetosphere. This conclusion is also supported by Streltsov and Pedersen (2011), who showed with 3-D MHD simulations that some luminous structures (in particular, rings and solid spots) produced by HAARP in the O-heating experiments can be interpreted in terms of ULF waves and FACs.

In this paper, we make the next step in the development of the numerical model used by Streltsov and Pedersen (2011) by including the Hall conductivity in the ionosphere and using a more realistic heating
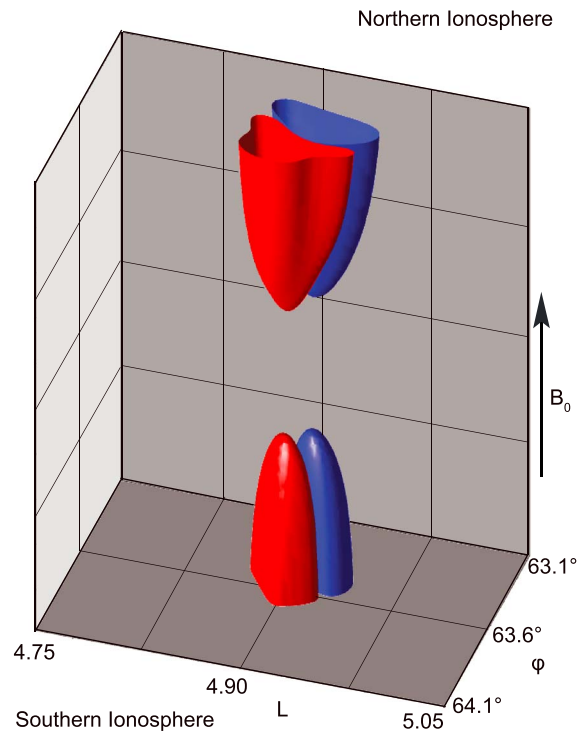
Figure 6. Snapshot of the parallel current density $j_\parallel$ taken from the 3-D simulation at $t = 158.5$ s with $\Sigma_H / \Sigma_P = 2$. Here isosurfaces of $j_\parallel = -0.002$ $\mu A/m^2$ (blue) and $j_\parallel = 0.002$ $\mu A/m^2$ (red) are shown.

mechanism. Namely, the model assumes that the heating decreases the recombination coefficient in the ionospheric E region, and the decrease in the recombination increases the density. We apply the model to the geomagnetic conditions observed during the experiment, and the results of the simulations are shown in Figures 6 and 7.

Specifically, in our simulation, the heating changes the plasma density in the E region in the Northern Hemisphere according to equation (4). Modification of the ionospheric density changes the conductivity, which generates FACs, if the large-scale electric field exists in the ionosphere (see equation (5)). Figure 6 shows a snapshot of the field-aligned current density inside the 3-D domain at the time $t = 158.5$ s after the heating has begun. In full agreement with Streltsov and Pedersen (2011), the simulations demonstrate that such constant heating leads to a rapid formation of two FACs that are closed through the ionosphere in both hemispheres. The structure of the currents obtained in our simulations is different from the structure of currents shown by Streltsov and Pedersen (2011). Namely, in our simulations, the heating produces two current channels standing side by side, and in the simulations by Streltsov and Pedersen (2011), the currents form an axisymmetric structure. This difference is explained by the different models for the heating used in these two studies.

The FAC flows from the Southern Hemisphere to the Northern Hemisphere in one channel (shown with red in Figures 6 and 7) and flows in the opposite direction along the adjacent channel (shown with blue). We assume that these FACs may cause some parallel electric field in the current channels (due to the dispersive effect, double layer formation, anomalous resistivity, or any other mechanisms that depend on the amplitude and the transverse size of FAC), which can accelerate electrons into the ionosphere and produce artificial aurora.

Figure 7 shows snapshots of the parallel current density and the plasma density in the ionosphere at $t = 158.5$ s. Specifically, Figures 7a and 6c show plasma and current densities produced by the heating in the ionosphere with $E_\perp = 6.5$ mV/m, $\Sigma_P = 0.4$ mho, and $\Sigma_H = 2\,\Sigma_P$. Figures 7b and 7d show plasma and current densities produced by the heating in the ionosphere with $E_\perp = 6.5$ mV/m, $\Sigma_P = 0.4$ mho, and $\Sigma_H = 0$ (no Hall current). The contour lines from Figures 7a and 7c are also shown in Figures 7b and 7d, to
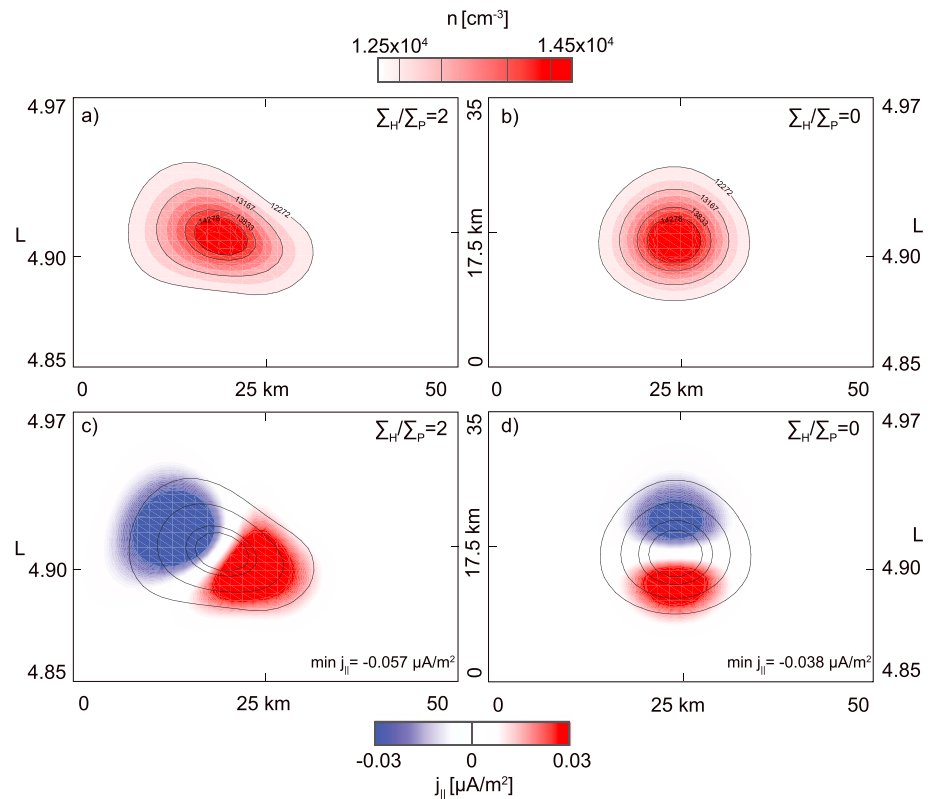
Figure 7. (a, b) Snapshots of ionospheric density n from the numerical model at $t = 158.5$ s under different ionospheric conditions: (a) with $\Sigma_H/\Sigma_P = 2$ and (b) with $\Sigma_H/\Sigma_P = 0$. (c, d) The snapshots of ionospheric $j_\parallel$ at $t = 158.5$ s with $\Sigma_H/\Sigma_P = 2$ and $\Sigma_H/\Sigma_P = 0$, respectively. The 3-D simulations are performed with $E_\perp = 6.5$ mV/m. The contour lines from panels (a) and (c) are mapped to panels (b) and (d) correspondingly, to demonstrate the relation between density enhancements produced by the heating and the structure and location of the corresponding field-aligned currents.

demonstrate relation between density enhancements produced by the heating and the structure and location of the corresponding FACs.

Figure 7 demonstrates that there are two important effects associated with adding a Hall conductivity into the model. First, the Hall conductivity increases the magnitude of the generated FAC by 50%. This result follows directly from equation (5). Second, the Hall conductivity rotates the FAC system around the center of the heating spot. This is in the agreement with equation (5) which states that FACs are generated in the direction of the resultant ionospheric conductivity (Jia & Streltsov, 2014). This happens because the FAC is closed through the ionosphere by the combination of Pedersen and Hall currents. The Pedersen current is parallel to the background electric field, which is in the north-south direction in our simulations, and the Hall current is perpendicular to it. Therefore, when the Hall conductivity is equal to zero, the field-aligned current is closed by the Pedersen current only, and this current is aligned with the electric field in the direction from $L = 4.75$ to $L = 5.05$. When the Hall conductivity is 2 times larger than the Pedersen conductivity, FACs are closed in the ionosphere at some angle to the direction of the background electric field.

Another interesting effect observed in the simulations is that the maximum of the downward (red) and upward (blue) field-aligned currents do not coincide with the maximum of the density disturbances or the maximum of the heating power. This happens because the currents are formed by the gradients in $\left(\Sigma_P \mathbf{E}_\perp + \Sigma_H \mathbf{E}_\perp \times \mathbf{b}\right)$ (see equation (5)), and when the background electric field is uniform, these gradients are produced by the density gradients only. Therefore, simulations predict that when the large-scale electric field in the ionosphere is relatively uniform, the bright luminous spot produced by the heating should be observed not exactly where the heating has a maximum power but in the close vicinity. The exact location and the orientation of the luminous structure relative to the heating spot and the orientation of the background electric field depend on the relation between Pedersen and Hall conductivities. This conclusion is

consistent with the observations which frequently show some offset between the heating and the maximum of the luminosity in heating experiments (Grach et al., 2016; Pedersen et al., 2009).

The reasonable agreement between the observations and results of 3-D simulations led us to conclude that the luminous spots and disturbances in the magnetic field detected during the 12 March 2013 HAARP experiment may be related to the magnetic FACs produced by the heating of the ionosphere with the X-mode HF waves. At the same time, we would like to emphasize that the complete physical model of the coupled and rapidly changing magnetosphere-ionosphere system during X-mode or O-mode heating is much more complicated and includes many physical effects which are not taken into account in our model. In particular, our model does not resolve the vertical structure of the ionospheric E region and does not include any electrochemistry of photoionization mechanism in the ionosphere. It also does not include any mechanisms producing the parallel electric field in the FACs in the magnetosphere, as well as the effects of the electron precipitation in the upward currents on the ionospheric density. Therefore, we think that more advanced and comprehensive models of the ionosphere-magnetosphere system are required to unambiguously explain the results from this particular experiment.

However, we also think that the generation of the FACs by the changing of the ionospheric conductivity in the presence of the large-scale electric field in the ionosphere is one of the most basic and robust results produced by the heating, and these FACs will always contribute to the energization of the ionosphere by delivering Poynting and particle fluxes into it. Hence, we conclude that the mechanism considered in this paper should always be taken into account together with other (local ionospheric) mechanisms in the experiments involving artificial modification of the ionosphere (particularly in the D and E regions).

5. Conclusion

In conclusion, we present results from the 12 March 2013 HAARP experiment, where the ionosphere was heated with the X-mode HF waves and bright luminous spots in the ionosphere were observed together with the disturbances of the magnetic field on the ground. We demonstrate with 3-D MHD simulations that these effects are consistent with the structure and dynamics of the magnetic FACs generated by the variation in the ionospheric density when the large-scale electric field exists in the ionosphere. Simulations reveal that the X-mode heating of the ionosphere generates FACs with maximum intensity shifted relative to the center of the heating spot, as was observed in many experiments. We investigated effects of the Hall conductivity on the structure of the generated currents: the simulations reveal that Hall conductivity (1) increases the amplitude of the generated FACs and (2) changes the location and the orientation of the current flowing into the ionosphere relative to the direction of the background electric field. Results from our 3-D simulations show a reasonable agreement with the observations. The main conclusion from our work is that the FACs certainly contribute to the total energization of the ionosphere and should be taken into account together with other, pure ionospheric mechanisms, to explain results of experiments involving modification of the ionospheric D and E regions.

References

Bernhardt, P., Duncan, L., & Tepley, C. (1988). Artificial airglow excited by high-power HF waves. *Science*, *242*, 1022–1027. https://doi.org/10.1126/science.242.4881.1022

Bernhardt, P., Tepley, C., & Duncan, L. (1989). Airglow enhancements associated with plasma cavities formed during ionospheric heating experiments. *Journal of Geophysical Research*, *94*, 9071–9092. https://doi.org/10.1029/JA094iA07p09071

Blagoveshchenskaya, N. F., Borisova, T. D., Yeoman, T. K., Haggstrom, I., & Kalishin, A. S. (2015). Modification of the high latitude ionosphere F region by X-mode powerful HF radio waves: Experimental results from multi-instrument diagnostics. *Journal of Atmospheric and Solar-Terrestrial Physics*, *135*, 50–63. https://doi.org/10.1016/j.jastp.2015.10.009

Blagoveshchenskaya, N. F., Kornienko, V. A., Borisova, T. D., Thide, B., Kosch, M. J., Rietveld, M. T., et al. (2001). Ionospheric HF pump wave triggering of local auroral activation. *Journal of Geophysical Research*, *106*(A12), 29071–29089. https://doi.org/10.1029/2001JA900002

Cohen, M. B., Inan, U. S., Golkowski, M. A., & McCarrick, M. J. (2010). ELF/VLF wave generation via ionospheric HF heating: Experimental comparison of amplitude modulation, beam painting, and geometric modulation. *Journal of Geophysical Research*, *115*, A02302. https://doi.org/10.1029/2009JA014410

Fenrich, F. A., Samson, J. C., & Sofko, G. (1995). ULF high- and low-m field line resonances observed with the Super Dual Auroral Radar Network. *Journal of Geophysical Research*, *100*(A11), 21535–21547. https://doi.org/10.1029/95JA02024

Getmantsev, G., Zuikov, N., Kotik, D., Mironenko, L., Mityakov, N., Rapoport, V., et al. (1974). Combination frequencies in the interaction between high-power short-wave radiation and ionospheric plasma. *ZHETF Pis'ma v Redaktsiiu*, *20*, 101–102.

Goertz, C. K., & Boswell, R. W. (1979). Magnetosphere-ionosphere coupling. *Journal of Geophysical Research*, *84*(A12), 7239–7246. https://doi.org/10.1029/JA084iA12p07239

Golkowski, M., Cohen, M. B., Carpenter, D. L., & Inan, U. S. (2011). On the occurrence of ground observations of ELF/VLF magnetospheric amplification induced by the HAARP facility. *Journal of Geophysical Research*, *116*, A04208. https://doi.org/10.1029/2010JA016261

Golkowski, M., Inan, U. S., Gibby, A. R., & Cohen, M. B. (2008). Magnetospheric amplification and emission triggering by ELF/VLF waves injected by the 3.6 MW HAARP ionospheric heater. *Journal of Geophysical Research*, *113*, A10201. https://doi.org/10.1029/2008JA013157

Grach, S., Sergeev, E., Mishin, E., & Shindin, A. (2016). Dynamic properties of ionospheric plasma turbulence driven by high-power high-frequency radiowaves. *Physics-Uspekhi*, *59*, 1091–1128. https://doi.org/10.3367/UFNe.2016.07.03786

Guido, T., Tulegenov, B., & Streltsov, A. V. (2014). Large-amplitude ULF waves at high latitudes. *Journal of Atmospheric and Solar-Terrestrial Physics*, *119*, 102–109. https://doi.org/10.1016/j.jastp.2014.07.006

Gurevich, A. (1978). *Nonlinear phenomena in the ionosphere*. New York: Springer-Verlag.

Gurevich, A. (2007). Nonlinear effects in the ionosphere. *Physics-Uspekhi*, *50*(11), 1091. https://doi.org/10.1070/PU2007v050n11 ABEH006212

Hasegawa, A. (1976). Particle acceleration by MHD surface wave and formation of aurora. *Journal of Geophysical Research*, *81*(28), 5083–5090. https://doi.org/10.1029/JA081i028p05083

Honary, F., Borisov, N., Beharrell, M., & Senior, A. (2011). Temporal development of the magnetic zenith effect. *Journal of Geophysical Research*, *116*, A06309. https://doi.org/10.1029/2010JA016029

Jasperse, J. R., Basu, B., Lund, E. J., & Grossbard, N. (2010). The self-consistent parallel electric field due to electrostatic ion-cyclotron turbulence in downward auroral-current regions of the Earth's magnetosphere. *Physics of Plasmas*, *17*(062904). https://doi.org/10.1063/1.3443713

Jia, N., & Streltsov, A. V. (2014). Ionospheric feedback instability and active discrete auroral forms. *Journal of Geophysical Research: Space Physics*, *119*, 2243–2254. https://doi.org/10.1002/2013JA019217

Kosch, M., Pedersen, T., Hughes, J., Marshall, R., Gerken, E., Senior, A., et al. (2005). Artificial optical emissions at HAARP for pump frequencies near the third and second gyroharmonic. *Annals of Geophysics*, *23*, 1585–1592. https://doi.org/10.5194/angeo-23-1585-2005

Kosch, M., Pedersen, T., Mishin, E., Oyama, S., Hughes, J., Senior, A., et al. (2007). Coordinated optical and radar observations of ionospheric pumping for a frequency pass through the second electron gyroharmonic at HAARP. *Journal of Geophysical Research*, *112*, A06325. https://doi.org/10.1029/2006JA012146

Mishin, E., Burke, W., & Pedersen, T. (2004). On the onset of HF-induced airglow at magnetic zenith. *Journal of Geophysical Research*, *109*, A02305. https://doi.org/10.1029/2003JA010205

Mishin, E., Burke, W., & Pedersen, T. (2005). HF-induced airglow at magnetic zenith: Theoretical considerations. *Annals of Geophysics*, *23*, 47–53. https://doi.org/10.5194/angeo-23-47-2005

Mishin, E., Watkins, B., Lehtinen, N., Eliasson, B., Pedersen, T., & Grach, S. (2016). Artificial ionospheric layers driven by high-frequency radiowaves: An assessment. *Journal of Geophysical Research: Space Physics*, *121*, 3497–3524. https://doi.org/10.1002/2015JA021823

Mozer, F. S. (1976). Anomalous resistivity and parallel electric fields. In B. M. McCormac (Ed.), *Magnetospheric particles and fields astrophysics and space science library (A Series of Books on the Recent Developments of Space Science and of General Geophysics and Astrophysics Published in Connection with the Journal Space Science Reviews)*, (Vol. 58, pp. 125–136). Dordrecht: Springer. https://doi.org/10.1007/978-94-010-1503-5_12

Nakamura, T. K. (2000). Parallel electric field of a mirror kinetic Alfven wave. *Journal of Geophysical Research*, *105*(A5), 10729–10737. https://doi.org/10.1029/1999JA900494

Papadopoulos, K., Wallace, T., McCarrick, M., Milikh, G. M., & Yang, X. (2003). On the efficiency of ELF/VLF generation using HF heating of the auroral electrojet. *Plasma Physics Reports*, *29*, 561–565. https://doi.org/10.1134/1.1592554

Pedersen, T., Gustavsson, B., Mishin, E., Kendall, E., Mills, T., Carlson, H. C., & Snyder, A. L. (2010). Creation of artificial ionospheric layers using high-power HF waves. *Geophysical Research Letters*, *37*, L02106. https://doi.org/10.1029/2009GL041895

Pedersen, T., Gustavsson, B., Mishin, E., MacKenzie, E., Carlson, H. C., Starks, M., & Mills, T. (2009). Optical ring formation and ionization production in high-power HF heating experiments at HAARP. *Geophysical Research Letters*, *36*, L18107. https://doi.org/10.1029/2009GL040047

Rietveld, M. T., Kosch, M. J., Blagoveshchenskaya, N. F., Kornienko, V. A., Leyser, T. B., & Yeoman, T. K. (2003). Ionospheric electron heating, optical emissions and striations induced by powerful HF radio waves at high latitudes: Aspect angle dependence. *Journal of Geophysical Research*, *108*(A4), 1141. https://doi.org/10.1029/2002JA009543

Robinson, T. R., Bond, G., Eglitis, P., Honary, F., & Rietveld, M. T. (1998). RF heating in a strong auroral electrojet. *Advances in Space Research*, *21*(5), 689–692. https://doi.org/10.1016/S0273-1177(97)01004-1

Samson, J. C., Wallis, D. D., Hughes, T. J., Greutzberg, F., Ruohoniemi, J. M., & Greenwald, R. A. (1992). Substorm intensifications and field line resonances in the nightside magnetosphere. *Journal of Geophysical Research*, *97*, 8495–8518. https://doi.org/10.1029/91JA03156

Stasiewicz, K., Bellan, P., Chaston, C., Kletzing, C., Lysak, R., Maggs, J., et al. (2000). Small scale Alfvénic structure in the aurora. *Space Science Reviews*, *92*, 423–533.

Streltsov, A. V. J.-J., Chernyshov, A. A., Frolov, L. V., Honary, F., Kosch, M. J., McCoy, R. P., et al. (2018). Berthelier Past, present and future of active radio frequency experiments in space. *Space Science Reviews*, *214*, 118. https://doi.org/10.1007/s11214-018-0549-7

Streltsov, A., Jia, N., Pedersen, T., Frey, H., & Donovan, E. (2012). ULF waves and discrete aurora. *Journal of Geophysical Research*, *117*, A09227. https://doi.org/10.1029/2012JA017644

Streltsov, A., Lotko, W., & Milikh, G. (2005). Simulations of ULF field-aligned currents generated by HF heating of the ionosphere. *Journal of Geophysical Research*, *110*, A04216. https://doi.org/10.1029/2004JA010

Streltsov, A. V., & Pedersen, T. R. (2011). Excitation of zero-frequency magnetic field-aligned currents by ionospheric heating. *Annales Geophysicae*, *29*, 1147–1152. https://doi.org/10.5194/angeo-29-1147-2011

Stubbe, P., & Kopka, H. (1977). Modulation of the polar electrojet by powerful HF waves. *Journal of Geophysical Research*, *82*(16), 2319–2325. https://doi.org/10.1029/JA082i016p02319

Stubbe, P., Kopka, H., & Dowden, R. L. (1981). Generation of ELF and VLF waves by polar electrojet modulation: Experimental results. *Journal of Geophysical Research*, *86*(A11), 9073–9078. https://doi.org/10.1029/JA086iA11p09073